In Vitro Electrochemical Measurement of Serotonin Release in the Human Jejunum Mucosa using a Diamond Microelectrode

SCHOLARONE™
Manuscripts

ARTICLE

In Vitro Electrochemical Measurement of Serotonin Release in the Human Jejunum Mucosa using a Diamond Microelectrode

Marion France[a], James J. Galligan[b,c], and Greg M. Swain[a,c]

We report herein on the use of a boron-doped diamond microelectrode (DME) to record oxidation currents *in vitro* associated with the release of serotonin from enterochromaffin cells in the epithelium of the human intestinal mucosa. Continuous amperometric measurements were made as a function of distance (ln current vs. distance) from the tissue surface in human jejunum specimens. The results demonstrate the capabilities of the DME for the stable and reproducible detection of serotonin in the complex environment of the human tissue. Serotonin release was evoked by the shearing force of a continuously flowing Krebs buffer solution at 36 ^{o}C with the tissue pinned down in a flow bath. Reproducible currents with distance were recorded for serotonin oxidation. Increased oxidation currents were observed in the presence of the selective serotonin transporter antagonist, fluoxetine, indicating that a significant fraction of the amperometric current recorded is attributable to serotonin oxidation. The nominal $|\text{slope}^{-1}|$ of the ln current vs. distance plots increased from 270 ± 25 μm^{-1} in Krebs buffer (N = 3) to 471 ± 65 μm^{-1} during fluoxetine addition (N = 3), reflective of a reduced rate of reuptake in the presence of the SERT antagonist. The paper reports on the characterization of the diamond microelectrodes and the *in vitro* electrochemical measurement data.

1. Introduction

Since the initial publications on the electrochemical properties of boron-doped diamond electrodes and their introduction for use in electroanalysis[1-4], the field has undergone significant growth over the past 20 years. The outstanding properties of this unique carbon material include (i) low and stable background current that is generally pH independent due to the relative absence of ionizable surface carbon-oxygen functional groups, (ii) stable film morphology and microstructure, (iii) resistance to molecular adsorption and biofouling, and relatively rapid electron-transfer kinetics for multiple redox systems in aqueous[4-9], organic[10,11] and ionic liquid[12,13] electrolyte media. Today, boron-doped diamond electrodes are available from multiple commercial sources placing them within reach of investigators for use. Conducting diamond electrodes can be prepared as thin films on a suitable substrate, free-standing plates, microelectrodes, microelectrode arrays, and conducting powders. In recent years, there have been several comprehensive reviews on diamond electrodes and current applications in neurochemical analysis.[14-16]

Diamond microelectrodes (DMEs) are suitable materials for neurochemical analysis *in vitro* and *in vivo* in both the peripheral and central nervous systems.[14-16] However, measurements made with DMEs tend to be *in vitro* rather than *in vivo*, as is customary with carbon fiber microelectrodes and investigations of neurochemical signalling in the brain.[17]

Our group has demonstrated in *in vitro* continuous amperometric measurements that DMEs provide a reproducible, stable, and sufficiently sensitive oxidation current response for norepinephrine released from sympathetic nerves innervating the arteries and veins of rats and mice[18-20], and serotonin (5-hydroxytryptamine, 5-HT)[21-24] and nitric oxide[25] in the small intestine and colon of guinea pigs, rats, and mice. The ability to stably detect serotonin released from enterochromaffin (EC) cells lining the epithelial layer of

[a.] Department of Chemistry, Michigan State University, East Lansing, MI 48824 USA.
[b.] Department of Pharmacology and Toxicology, Michigan State University, East Lansing, MI 48824 USA .
[c.] Neuroscience Program, Michigan State University, East Lansing, MI 48824 USA.

the gastrointestinal (GI) mucosa or from interneurons in the gut wall using DMEs is noteworthy that this analyte is a widely recognized carbon electrode biofouling agent. The biofouling that plagues carbon fiber microelectrodes does not occur on diamond microelectrodes to any appreciable extent. Biofouling results from serotonin oxidation that involves the formation of interfacial reaction products that adsorb onto the electrode surface and reduce the number of electroactive sites available for subsequent serotonin molecule oxidation. Therefore, a rapid decrease in the electrode response sensitivity is observed.[26-30] Carbon fiber microelectrodes are susceptible to biofouling because the sp^2-hybridized carbon microstructure possesses an extended pi-electron system, and the electrode surface is highly covered with carbon-oxygen functional groups. Serotonin oxidation reaction products adsorb strongly to the polar surface by hydrogen-bonding, ion-dipole, and dipole-dipole interactions with the pi electrons and the surface carbon-oxygen functional groups.[3,31] In contrast, DMEs are sp^3-hybridized with no extended pi-electron system and are devoid of high surface coverages of carbon-oxygen functional groups after deposition or hydrogen plasma treatment (e.g., generally < 0.03 % O/C).[32,33]

Some of the more recent applications of DMEs in neurochemistry and neurophysiology are summarized here. Researchers have begun to use DMEs and diamond microelectrode arrays to interface with neuronal cell cultures for the purpose of measuring action potentials and applying electrical stimulation.[34,35] The high charge injection, hardness and durability, stable surface chemistry and microstructure, and biocompatibility of the material are attractive properties. *In vivo* detection of dopamine[36-39] and serotonin[40] using DMEs has been reported as has the study of the real time metabolism of the drug, methyl cobalamin, at two distinct locations in the cochlea and leg muscle of live guinea pigs.[41] Fierro et al. described the *in vitro* measurement of glutathione released from human cancer cells in culture using a DME.[42] Other researchers have reported on the preparation of a flexible diamond microelectrode for neurochemical measurements[43] and on the fouling resistance of DMEs during neurochemical measurements using fast scan cyclic voltammetry.[44,45]

We expand the application of DMEs in neurochemistry and report on their use, along with an electrode approach curve measurement protocol developed by Marcelli and Patel[46,47], to study serotonin release and uptake dynamics in the mucosa of the human jejunum. Serotonin is an important neurochemical signalling molecule in the GI tract where the majority of total body content is stored and released from EC cells that line the intestinal mucosa.[48,49] In the EC cell, serotonin is synthesized from tryptophan by tryptophan hydroxylase 1 (TPH1).[48,49] EC cells are pressure receptors (i.e., responding to movement of intestinal content) and release serotonin into the lamina propria where it activates its receptors localized on intrinsic primary afferent nerve fibers initiating peristaltic and secretory reflexes.[50] Serotonin also activates extrinsic primary afferent neurons to transmit information to the central nervous system.[51] The neurotransmitter's actions are terminated through uptake into neighboring enterocytes by the serotonin reuptake transporter (SERT).

We report herein on the *in vitro* continuous amperometric measurement of serotonin overflow from the mucosa of the human jejunum. It is demonstrated that (i) DMEs provide a reproducible and stable oxidation current with time in the human tissue and (ii) local serotonin levels can be manipulated through the addition of a serotonin uptake transporter antagonist, fluoxetine. The innovative aspects of the work are two-fold. First, as compared to the brain and central nervous system, there has been little work on the use of electrochemical methods and new electrode materials in the peripheral nervous system to better understand neurosignaling processes. Second, the work reports on the capabilities of diamond microelectrodes and electrochemical measurement protocols for the study neurosignaling processes in human tissue.

2. Experimental

2.1 Chemicals

All experiments were performed using oxygenated (95% O_2, 5% CO_2) Krebs buffer of the following composition: 117 mmol L^{-1} NaCl, 4.7 mmol L^{-1} KCl, 2.5 mmol L^{-1} $CaCl_2$, 1.2 mmol L^{-1} $MgCl_2$, 1.2 mmol L^{-1} NaH_2PO_4, 25 mmol L^{-1} $NaHCO_3$, and 11 mmol L^{-1} glucose. Stock serotonin solution aliquots (100 μmol L^{-1}) were used to prepare a 10 μmol L^{-1} solution in Krebs buffer for electrode testing prior to and after *in vitro* tissue exposure experiments. These characterization

ARTICLE

measurements were performed to probe for changes in oxidation peak potential and current that would be reflective of electrode fouling. Stock fluoxetine solution aliquots (100 µmol L^{-1}) were used to prepare a 1 µmol L^{-1} solution in Krebs buffer for tissue superfusion. Serotonin and fluoxetine stock solutions were stored at -20 ˚C. All analyte solutions in Krebs buffer were prepared fresh prior to an experiment. All chemicals were purchased from Sigma-Aldrich (St. Louis, MO, USA).

2.2 Boron-Doped Diamond Microelectrode (DME) Preparation.

Pt wire (99.99 %, Sigma-Aldrich, 76 and 40 µm diameter) was cut into a 1.3 cm long segment. Both ends were sharpened into a conical shape by electrochemical etching in 1 M KOH.[21-24,51-54] The sharpened Pt wire was ultrasonically cleaned in acetone for 10 min and then ultrasonically seeded in a diamond powder suspension (3–6 nm particles, ca. 20 mg in 100 mL of ethanol, Tomei Diamond Co., Tokyo, Japan) for 30 min. A thin film of boron-doped diamond was deposited on the seeded Pt wire using microwave plasma-assisted chemical vapor deposition (CVD). It is common practice to deposit boron-doped diamond on three to five Pt wires simultaneously. The deposition was performed using a commercial CVD system (1.5 kW, 2.54 GHz, ASTeX, Woburn, MA, USA) in which the source gas mixture was 0.5% CH_4/H_2 (v/v) with 10 ppm of diborane (0.1% B_2H_6 diluted in H_2) added for boron doping. The deposition parameters were as follows: microwave power = 600 W, system pressure = 45 Torr, and substrate temperature = 700 - 800 °C, as estimated using a disappearing filament optical pyrometer. The deposition time was 10 h. Afterward, each diamond-coated Pt wire was cut in half yielding two conically shaped DMEs. The cut end of each wire was affixed to a Cu wire using conducting Ag epoxy and super glue. The diamond-coated end of each wire was then insulated with polypropylene from a heated pipette tip.[53] This design is illustrated in Figure 1. The resulting DME was conical in shape with a tip ~5 µm in diameter, a cylindrical region ~80 µm wide (for the 76 µm diam. wire), and a typical exposed length of 300 - 600 µm. In this insulation process, the exposed DME length protruding from the melted pipet tip is difficult to precisely control.

2.3 Material Characterization

Scanning electron microscopy was performed at the Center for Advanced Microscopy (MSU) using a JSM-6610LV (JEOL USA) general purpose microscope. Accelerating voltages used were between 10-20 kV with a working distance 9 – 11 mm. Secondary electron micrographs are presented.

Raman spectroscopy was performed using a Renishaw inVia Reflex spectrometer. The instrument consisted of a confocal microscope connected to a continuous wave, diode-pumped solid-state laser (100 mW) with a fundamental emission at 532 nm. The sample was positioned under the laser light using a motorized stage. The stage position was controlled, and spectral data acquired with commercial software (WiREInterface). This software allows for control over the laser power, exposure time, spectral range covered, and stage positioning for mapping a sample. The parameters used were a laser power of 10 mW at the sample and an integration time of 5 s. Each spectrum was generated from the average of 5 spectral acquisitions at each point. A Leica (100x/0.85 N.A.) objective lens was used for focusing the excitation light and collecting the scattered radiation. An 1800 lines mm^{-1} holographic grating was used.

2.4 Human Jejunal Specimens

All procedures using human tissues were approved by the Institutional Review Board at Michigan State University. Michigan State University (MSU) applies the ethical principles found in the Belmont Report (National Commission for the Protection of Human Subjects of Biomedical and Behavioral Research, 1979) to all of its activities related to human subject research, regardless of funding. All tissue specimens were obtained from patients undergoing gastric by-pass surgery who first provided signed consent. The researchers were blinded to any personal data that could identify the person from whom the tissue originated. The bariatric surgical procedure for weight loss was performed at Sparrow Hospital (Lansing, MI), approximately 5 miles from the Michigan State University campus. Intestinal specimens surgically removed were immediately placed in cold Krebs buffer solution and transported shortly thereafter to campus. Once received (30-60 min after removal), the connective and adipose tissues were cut away from the intestine using small spring scissors (Fine Science Tools, Foster City, CA, USA). A segment (ca. 1 cm) of the jejunum was then sectioned and carefully cut open

with fine scissors along the segment length. The cut specimen was then opened (~ 1 cm^2), gently stretched, and pinned down flat (stainless steel, 0.2 mm diameter, 26002-20, Fine Science Tools, Foster City, CA, USA) in a Sylgard®-lined flow bath (vol. = ~ 6 mL) with the mucosa facing upward and exposed. During this dissection, the tissue appearance, including color and villus integrity, were visually evaluated. Experiments were only performed with tissues that were a healthy-looking color (pale color of the peach fruit) and the mucosa was not visibly sloughing off. Oxygenated Krebs buffer solution at room temperature flowed over the tissue at a rate of 2 mL min^{-1} controlled by a peristaltic pump (Minipuls 2, Gilson, Middleton, WI, USA). DME positioning near the villus was accomplished using an upright optical microscope (Model SMZ1000, Nikon, USA). Experiments commenced after a 30 min equilibration period with the mounted tissue specimen exposed to flowing Krebs buffer at room temperature. All electrochemical measurements were performed with the flow bath, microscope, and stage shielded within a Faraday cage to minimize pick-up of extraneous electrical noise.

2.5 Cyclic Voltammetric and Continuous Amperometric Measurements.

A three-electrode configuration was used for the electrochemical measurements prior to and after the *in vitro* measurements with the DME working electrode. A Pt wire counter electrode and a lab-made Ag/AgCl (3M KCl) reference electrode completed the cell. The measurements were performed using a Model 650 A electrochemical workstation (CH Instruments, Austin, TX, USA). For basic DME characterization, a single compartment glass electrochemical cell (~ 25 mL) was used. Cyclic voltametric curves were recorded in a 10 µmol L^{-1} serotonin solution, prepared with Krebs buffer, over the potential range from -0.2 to 1 V at scan rates from 0.1 - 250 V s^{-1}. Oxidation peak potentials and peak currents were determined and assessed to verify DME quality and activity.

Continuous amperometry (CA) was used to study the dynamics of serotonin release and uptake *in vitro* at the mucosal surface of the human jejunum. A potential of 0.8 V vs. Ag/AgCl was applied to a DME placed near the mucosal surface to measure serotonin overflow in the extracellular solution as an oxidation current using a ChemClamp potentiostat (Dagan Corp., Minneapolis,

MN, USA). The applied detection potential for a given DME was determined from cyclic voltametric measurements (described above). At the detection potential, serotonin molecules are oxidized at a mass transfer limited rate arriving from nearby release sites on villi (i.e., EC cells). Release of 5-HT was evoked by the mechanical action of the superfusing Krebs buffer. DMEs have been previously shown to exhibit a sufficiently sensitive, reproducible, and stable serotonin oxidation potential and current in animal model tissues *in vitro*.[21-24] In the *in vitro* measurements, a two-electrode arrangement was used with a lab-made Ag/AgCl (3M KCl) electrode serving as both the counter and reference electrode. The reference electrode was positioned in the flow bath away from the tissue specimen near the exit port.

The CA measurements were performed as current approach curves in which the electrode distance from the mucosal surface was decreased in a stepwise fashion from 2000 to 50 µm using a precision micromanipulator. This procedure was first reported by Marcelli and Patel[46,47] and has been used by our group in prior reports.[21-24] These electrode distances were chosen because tissue topological-dependent errors were minimal in this range of electrode distances.[46] To determine the distance of the electrode from the mucosal surface, the electrode was first positioned (zero calibration) by gently touching the villus and then was retracted to 2000 µm. The touch point of the tissue was observed with an optical microscope, and given the limitation in resolution, there is some uncertainty in assigning the actual "zero point" for the distance approach curves. The 2000 µm distance was used for assessing the background current. Current approach curves commenced once the current at this distance was stable. The electrode was positioned at each electrode distance for approx. 40-60 s until the amperometric current stabilized. In our studies, serotonin uptake was assessed by comparing the reciprocal of the slope, $\left|\mathbf{slope^{-1}}\right|$, derived from the linear fit of the ln (current) vs. electrode distance plot.[46,47] An increase in the $\left|\mathbf{slope^{-1}}\right|$ value is reflective of reduced serotonin uptake.[46,47] Fluoxetine (1 µmol L^{-1}), a selective serotonin reuptake inhibitor (SSRI), was used to probe for SERT function. Fluoxetine is not electroactive at the potentials used for serotonin oxidation, so it does not contribute

ARTICLE
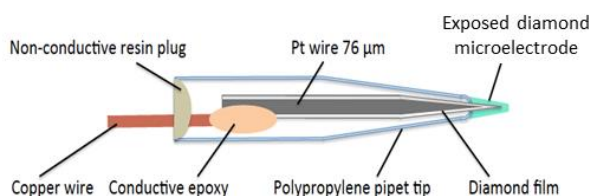
Figure 1. Illustration of the insulated diamond microelectrode design with a conically shaped electrode tip exposed outside of the polypropylene insulation.

to the current response (data not shown). The perfusing fluoxetine solution was applied to the tissue for at least 5 min prior to making any CA measurement. The typical measurement protocol for this study involved making CA measurements before exposing the tissue to fluoxetine, during the application of fluoxetine, and again after washout of the drug.

3. Results

3.1 Electrode Material Characterization

Figure 1 presents an illustration of how the conically shaped DMEs were prepared. One end of a diamond-coated Pt wire is affixed to a Cu wire using conducting Ag epoxy for the purpose electrical connection. A polypropylene pipet tip is carefully melted to insulate the diamond-coated Pt wire leaving a conically shaped cylinder exposed. The exposed conically shaped microelectrode
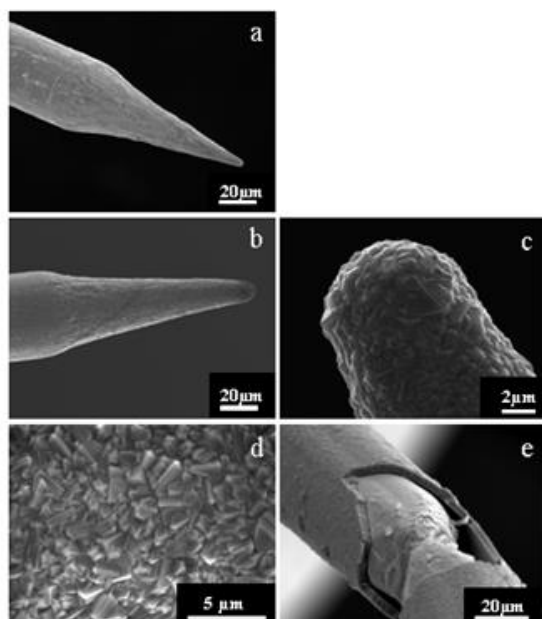
Figure 2. SEM micrographs of (a) an electrochemically-sharpened 40-µm diam. Pt wire, (b) a polycrystalline boron-doped diamond film coated 40-µm Pt wire, (c) the tip of a 40-µm Pt wire covered with polycrystalline diamond film, (d) the surface of polycrystalline diamond film deposited on the Pt wire, and (e) a damaged boron-doped diamond-coated 40 µm diam. Pt wire.

is formed on the sharpened end of the Pt wire substrate. It is difficult to control the length of the exposed DME using this insulation method. The exposed tip diameter is several micrometers while the exposed length varies from 300-600 µm generally.

Figure 2a shows an SEM micrograph of a 40 µm rather than 76 µm diam. Pt wire after electrochemical etching, but prior to diamond deposition. We have previously reported microscopy data for 76 µm Pt wires coated with polycrystalline diamond.[18-20,53-55] The conical electrode shape is evident with a radius of tip curvature of < 4 µm. Figure 2b shows a micrograph of a sharpened Pt wire covered by a film of polycrystalline diamond. Complete film coverage is typical based on micrographs for multiple microelectrodes. The reason Pt was selected for use as the substrate is because if there is incomplete coverage or defects in the diamond film through which solution can reach the metal, then a voltammetric signature for Pt will be evident. Background cyclic voltammograms for the microelectrodes in acid will exhibit currents for H_2 evolution at much lower overpotential than is observed for diamond, if there is exposed Pt due to cracks, delamination or incomplete diamond film coverage. The polycrystalline diamond film is rough and faceted, as evident in the higher magnification micrographs presented in Figure 2c and d. The tip radius after coating increases to slightly over 5 µm. The micrograph in Figure 2e shows a particular microelectrode where some film delamination occurred. Delamination is not the norm but, in this case, it provided a means to determine the film thickness. Based on cross-section analysis, the film thickness is approximately 4 µm for the growth conditions employed.

Figure 3 presents a visible Raman spectrum for a
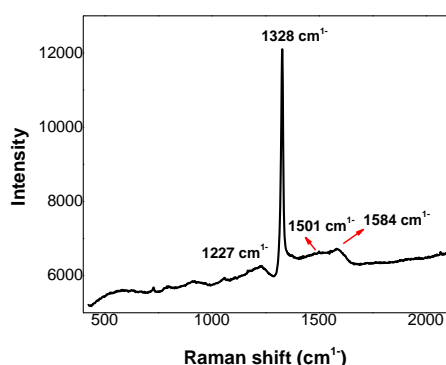
Figure 3. Visible Raman spectrum recorded from the surface of a diamond-coated Pt wire microelectrode. Excitation wavelength = 532 nm. Laser power at sample = 10 mW. Integration time per spectrum = 5 s.

polycrystalline, boron-doped diamond film deposited on a 76 μm diam. Pt wire. The spectrum for the polycrystalline film consists of a sharp and narrow first-order diamond phonon peak at 1328 cm^{-1} with very little scattering intensity in the 1500-1600 cm^{-1} region. The diamond linewidth (FWHM) is 11 cm^{-1}. Scattering in the 1500-1600 cm^{-1} region results when there is adventitious sp^2 bonded carbon impurity is present at or near the surface in grain boundaries or at the diamond-Pt interface.[53,55-57] There was little photoluminescent background observed with the visible excitation, also consistent with low levels of non-diamond carbon impurity. It should be noted that the scattering cross-section is larger for sp^2 carbon (*e.g.*, graphite) than for diamond, so the weak intensity at 1504 and 1584 cm^{-1} is consistent with low levels of non-diamond carbon impurity.[56-58]

3.2 Basic Electrochemical Properties

Figure 4 shows a representative cyclic voltammetric *i-E* curve for serotonin (5-HT, 10 μmol L^{-1}) prepared in Krebs buffer and a voltammogram recorded in the buffer alone. The electrode potential was scanned from -0.2 to 1 V at a rate of 0.1 V s^{-1}. The peak oxidation potential (E_p^{ox}) of 5-HT is ca. 0.60 V. At this potential and more positive ones, 5-HT molecules released from nearby EC cells are oxidized at a mass-transport controlled rate.

Figure 4. Cyclic voltammetric *i-E* curves for the background in Krebs buffer (pH 7.2) and 10 μmol L^{-1} serotonin (5-HT) + Krebs buffer at a typical diamond

thin film deposited on a sharpened 76 μm diam. Pt wire. The microelectrode was insulated with polypropylene, as illustrated in Figure 1. Scan rate = 0.1 V s^{-1}.
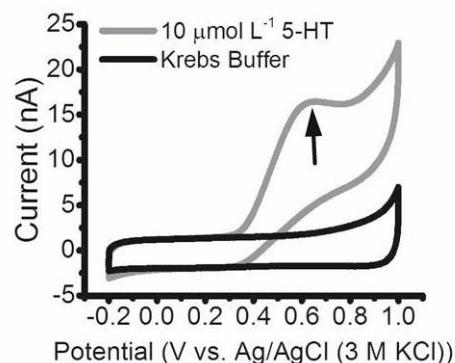
Table 1 presents a summary of the cyclic voltametric oxidation peak potential, E_p^{ox}, and/or peak potential separation, ΔE_p, values for dopamine (DA), norepinephrine (NE), and serotonin (5-HT) recorded using four different DMEs. We have previously reported similar data for different redox systems at DMEs formed on 76 μm diam. Pt wires at low scan rates (~0.1 V/s).[53-55] The data presented in the table are for a high scan rate of 250 V/s at DMEs formed on 40 μm diam. Pt wires. Well defined oxidation peaks, after background subtraction, were observed for all three analytes at this scan rate. 5-HT was the most easily oxidized (635 mV) of the three analytes, followed by DA (829 mV), and then NE (902 mV). The ΔE_p values for DA and NE were large, >1000 mV, indicative of slow charge-transfer kinetics at the diamond surface. Typically, the heterogeneous electron-transfer kinetics for catecholamines are more sluggish at diamond electrodes than at carbon fiber microelectrodes.[1,16,53,54,59] The reason for this is thought to be the absence of strong surface interactions (*i.e.*, adsorption) on diamond that lower the activation barrier for the electron transfer. The i_p^{ox} values for DA, NE and 5-HT were 150, 140 and 90 nA, respectively. The concentration of each analyte was 10 μM, but the microelectrodes used for the measurement of each had different exposed electrode geometric areas, which contributed to the variability in peak current values. These data reveal DMEs formed with the 40 μm diam. Pt wires have sufficient electrical conductivity and electrochemical activity to provide a useful response at high scan rates.

Table 1. Comparison of Cyclic Voltammetric E_p^{ox} and ΔE_p Data for Three Bioanalytes at Diamond Microelectrodes.

ARTICLE

Analyte	E_p^{ox}/mV	ΔE_p/mV
NE	902 ± 34	1048 ± 36
DA	829 ± 50	1035 ± 47
5-HT	635 ± 11	

Background-subtracted cyclic voltammetric *i-E* curves were recorded at 250 V/s in redox analyte solutions prepared with 0.1 M PB buffer (pH 7.4) recorded at diamond microelectrodes formed with 40 μm diam. Pt . The concentration of each analyte was 10 μM. The results presented are mean ± S.D. for four different microelectrodes.

3.3 *In Vitro* Continuous Amperometric Measurements

Figure 5A and B presents optical micrographs of the intestinal microvilli in the human jejunum at two slightly different magnifications. The microvilli are small, finger-like projections that extend into the lumen of the small intestine. These are coming out of the micrograph toward the viewer. Each villus is *ca.* 500 μm in length and has a diameter of *ca.* 200 nm. There is about 1 villus per cm^2 in this section of the jejunum specimen, based on the micrograph in Figure 5A. The microvilli increase the surface area of the epithelial cell-lined mucosal layer available for contact with lumenal content. These epithelial cells regulate functions like the absorption of water and nutrients into the bloodstream. Intestinal epithelial cells also mediate interactions between the mucosal immune system and lumenal materials.[48-50]
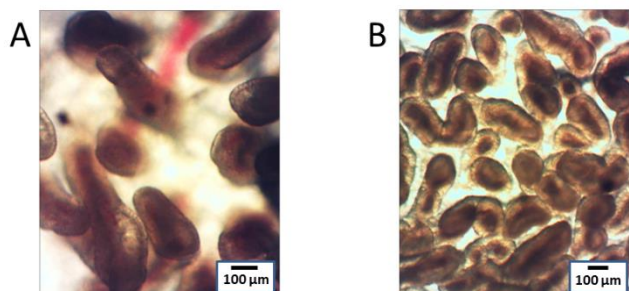
Figure 5. Plan-view optical micrographs displaying the microvilli of the human jejunum at two slightly different magnifications. A was collected at a slightly higher magnification than B. EC cells that release serotonin and enterocytes that express the serotonin uptake transporter (SERT) reside within the epithelial layer along the surface of the microvilli.

To gain information on the dynamics of serotonin release from EC cells and uptake by SERT expressed in neighboring enterocytes, current approach curves were recorded in the continuous amperometric (CA) measurement mode. Figure 6A presents a current approach curve (current versus tissue-electrode distance).
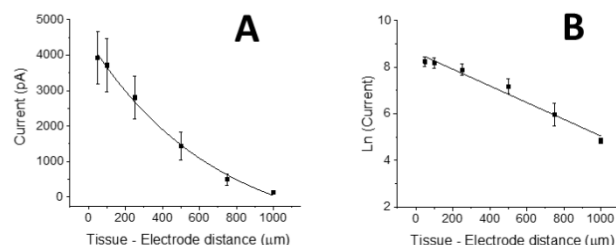
Figure 6. Current versus tissue-electrode distance plots in which the current magnitude for 5-HT oxidation plotted against a specific tissue-electrode distance was calculated from the difference in (A) current magnitude measured after 20-30 s at tissue-electrode distances from 2000-50 μm. (B) Natural log (ln) of the current magnitude in (A) plotted against increasing tissue-electrode distance. Data are mean ± S.E.M. N = 3 tissue specimens. Detection potential = 0.8 V vs. Ag/AgCl. The slope of the curve is -0.0036 μm^{-1} and the y-axis intercept is 8.63 (R^2 = 0.9691).

constructed by recording the amperometric current for 5-HT oxidation as a function of distance between the DME and the mucosal surface. Measurements were made at approximate distances of 2000, 1000, 750, 500, 250, 100, and 50 μm from the mucosa. The "zero distance" was established by gently touching the tissue, as observed with an optical microscope. As mentioned above, there is some uncertainty in this touch point, so the absolute distances reported in the figure, especially up close, have some uncertainty associated with them. The detection potential in these measurements, and all others reported herein, was 0.8 V vs. Ag/AgCl. At this potential, 5-HT is oxidized at a mass transfer limited rate. The approach curve in Figure 6A reveals that the oxidation current recorded after stimulation increases as the DME is positioned closer to the tissue surface. This is because the concentration of 5-HT in the nearby extracellular solution is highest at the tissue interface nearest the release sites. At distances far from the mucosal surface (*e.g.*, 2000 μm), the measured current is low because of dilution effects and similar in magnitude to the background current recorded in the absence of the tissue. The variability in the current data at each distance increases as the DME is positioned closer to the tissue. This variability is attributed to two factors: (i) uncertainty on the touch point distance with the micromanipulator from which all other distances

are measured, and (ii) the number of EC cells and enterocytes expressing SERT in the mucosal layer near the DME.

Figure 6B shows a plot of the natural log (ln) of the 5-HT oxidation current versus the tissue-DME distance. The plot displays an inverse linear relationship. The linear fit yields a slope and a vertical axis intercept, I_o. The slope of the curve is -0.0036 μm^{-1} and the y-axis intercept is 8.63 ($R^2 = 0.9691$). According to the model developed and originally tested by Marcelli and Patel[46,47], the reciprocal of the slope (absolute value), $|\mathbf{slope^{-1}}|$, is a measure of the rate of 5-HT reuptake by the serotonin reuptake transporter (SERT). The ratio between the y-axis intercept and the reciprocal of the slope, $I_o/|$slope$^{-1}|$ is a measure of the flux of 5-HT from nearby release sites and serves as a measure of the nominal release rate from EC cell nearby the DME position.

Figure 7 presents CA current-time curves recorded as a function of distance from the tissue. It is these types of measurements that are used to generate the data for the plots in Figure 6. The measurement records lumenal spillover of 5-HT released from EC cells. CA measurements have been previously reported using carbon fiber[61-63] and DMEs[21-24,46.47] in different animal intestinal tissues. Release is evoked by the shear force of the perfusing Krebs buffer. EC cells function as chemical and mechanical transducers. Mechanical forces can trigger 5-HT release under physiological conditions include tensile force and flow shear stress, intraluminal pressure, touch, and membrane distortion/deformation.[60] The oxidation current reaches a steady state at each distance within about 10 sec after
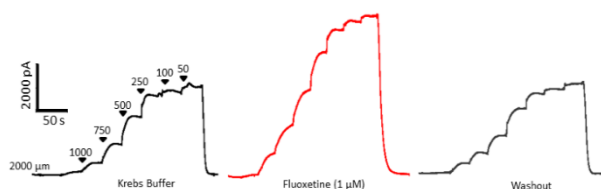
Figure 7. Continuous recordings of serotonin (5-HT) oxidation currents at varying electrode distances (2000 – 50 μm) of the DME with respect to the mucosa surface. Measurements were made before (Krebs buffer; pH = 7.4), during application, and after (washout) of the selective serotonin uptake inhibitor (SSRI), fluoxetine (1 μmol L^{-1}; 5 min), to determine if increases in current magnitude at each electrode distance were fluoxetine-dependent. Fluoxetine produced a reversible increase in serotonin oxidation currents. Detection potential = 0.8 V vs. Ag/AgCl.

a change in DME position. The measurements are typically made from far to closer distances. The current increases as the DME is positioned closer (1000-50 μm) to the mucosal surface because the concentration of 5-HT in the extracellular volume is greater nearest the tissue (*i.e.*, less dilution). Current approach curves are presented that were recorded initially in Krebs buffer and after washout of the drug, fluoxetine, in Krebs buffer (black curves) and in the presence of the drug (red curve) using the same tissue specimen. These before and after (black curves) current-time profiles have similar current magnitudes as a function of the DME distance illustrating the oxidation current response of the DME was stable throughout the course of the experiment. Following the initial current-distance approach curve recording, the SSRI, fluoxetine (1 μmol L^{-1}), was added to the continuously flowing Krebs buffer solution. As expected, this evoked an increase in the current magnitude at each electrode distance since 5-HT transporter-mediated reuptake is selectively blocked. This produces a greater concentration of the neurotransmitter in the extracellular solution at the DME. Increases in 5-HT oxidation currents during fluoxetine superfusion were reproducible in consecutive current approach curves (data not shown). Following, fluoxetine was removed during a washout period to determine if increases in the current magnitude observed in the presence of the drug were related to drug action. The current approach curves recorded after the washout period were consistent with the initial current magnitudes at each electrode distance before fluoxetine was applied, indicating the increased current at each electrode distance was fluoxetine dependent.

There was some variability in the current magnitude with distance in these measurements depending on where the DME was positioned across a tissue specimen. This is because, as mentioned above, at distances close to the mucosal surface, the measured oxidation current can be influenced by variability in the number of EC cells and enterocytes expressing SERT in the vicinity of the recording microelectrode. The measurements were made at so-called "hot spots" where robust 5-HT oxidation currents were measured initially. For this reason, the same region of a tissue specimen was used for the entire experimental series with and without a pharmaceutical manipulation.

ARTICLE
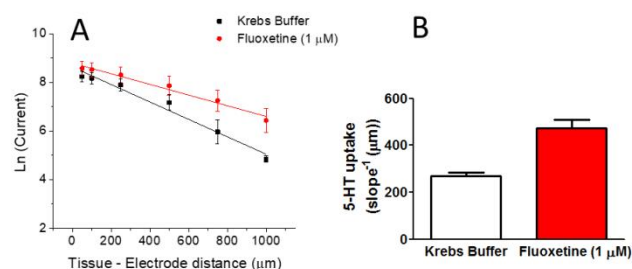
Figure 8. (A) Ln current (pA) versus distance plots of the serotonin oxidation current with and without fluoxetine (1 μmol L^{-1}). (B) Bar graphs of the aggregated data of curve slope with and without fluoxetine. Decreased serotonin clearance by SERT as shown by a decrease in the slope of the ln (current) versus tissue-electrode distance plot compared to Krebs buffer alone (control). Data are presented for mean ± S.E.M. for N=3 tissue specimens. Detection potential = 0.8 V vs. Ag/AgCl.

Figure 8A presents plots of the natural log (ln) value of the current versus the distance of the microelectrode away from the tissue surface in the presence and absence of fluoxetine (1 μmol L^{-1}). The nominal current decreases with increasing electrode-tissue distance in both Krebs buffer (black curve) and Krebs buffer plus the serotonin transporter antagonist, fluoxetine. The current magnitude plotted at each electrode distance was determined by averaging the measured current after 20 - 30 s post positioning of the DME at a particular distance and subtracting from this from the average background current recorded at 2000 μm. Linearity is observed in both plots, but the slope is less for the data recorded in the presence of fluoxetine. In Krebs buffer, the initial slope is -0.0036 ± 0.0003 (slope ± uncertainty) and the y-axis intercept is 8.63 ± 0.16 (R^2 = 0.9691). In the Krebs buffer plus fluoxetine solution, the slope is reduced to -0.0022 ± 0.0002 and the y-axis intercept is 8.79 ± 0.09 (R^2 = 0.9712). After drug wash out, at least in short-term measurements, the slope and y-axis intercept values were near the initial values. Marcelli and Patel's reaction-diffusion model was utilized to gain information on serotonin clearance by investigating the transporter-mediated reuptake independent of serotonin release.[46,47] In this model, the natural log (ln) of the current measurement at each electrode distance was determined and plotted against the electrode distance. The linear fit of the data was performed, and the reciprocal of the slope, $\left|\mathbf{slope^{-1}}\right|$, was determined to assess serotonin uptake, as previously described.[46,47]

SSRIs, such as fluoxetine, block serotonin reuptake by acting on SERT. If fluoxetine decreases the reuptake

rate, then the $\left|\mathbf{slope^{-1}}\right|$ value should be greater when the drug is applied relative to the drug-free control measurement. Figure 8A demonstrates there is a fluoxetine-dependent increase in the serotonin oxidation current as a function of distance (red versus black curve). The slope of the linear plots is less in the presence of the drug reflecting increased 5-HT concentration in the extracellular solution. The decreased slope results in an increase in the $\left|\mathbf{slope^{-1}}\right|$ value (Figure 8B). The nominal $\left|\mathbf{slope^{-1}}\right|$ increased from 270 ± 25 μm^{-1} in Krebs buffer (N = 3) to 471 ± 65 μm^{-1} during fluoxetine addition (N = 3). The ratio of the y-axis intercept, I_o, and the reciprocal of the slope, $I_o/\left|\mathbf{slope^{-1}}\right|$ is a measure of the flux at the tissue surface and reflects the 5-HT release rate.[46,47] The y-axis intercepts, I_o, were 5597 ± 2 pA (value ± uncertainty) in Krebs buffer (N=3) and 6568 ± 5 pA with fluoxetine addition (N=3). In terms of the $I_o/\left|\mathbf{slope^{-1}}\right|$ ratio, the nominal value is 21.3 ± 3.4 pA μm^{-1} in the presence of Krebs buffer and decreases to a nominal value of 14.1 ± 4.1 pA μm^{-1} in the presence of fluoxetine. These data are presented as mean ± std. dev. for N=3 different tissue specimens. The ratio in the presence of fluoxetine is statistically lower than the value in Krebs buffer (p = 0.026). An explanation for this difference is a possible feedback mechanism with autoreceptors expressed by EC cells activated by the greater level of 5-HT in the extracellular solution to decrease the release rate.[47,64,65] These results are consistent with those obtained in guinea pig ileum and colonic tissues.[46,47] Additionally, the oxidation current increase in the presence of the SERT antagonist indicates that the measured signal is arising, at least in part, from serotonin oxidation

A major advantage of DMEs compared to carbon fiber microelectrodes, specific to measurements in the serotonin-rich GI tract, is the resistance to biofouling during continuous exposure to the tissue constituents and serotonin oxidation reaction products.[21-24,59] Electrode biofouling decreases the electrode response and attenuates the amperometric current with time. There is likely some inherent fouling resistance due to the flowing Krebs buffer that is expected to sweep contaminants and oxidation reaction products away from the DME surface. To date, though, DMEs have been shown to remarkably operate stably in complex environments including the guinea pig GI mucosa for days and weeks, whereas the carbon fiber signal decreases within minutes.[21-24,59] Figure 9A

demonstrates that the DME provides a stable oxidation current response for serotonin with time at an electrode distance close to the mucosal layer of the human small intestine. The electrode was positioned 250 μm away where serotonin oxidation current is detectable. The neurotransmitter released from the nearby EC cells was evoked by the simple shear force of the flowing buffer across the tissue. The measured current remained stable for an extended period of time demonstrating that electrode fouling and thus loss of signal is not significant.[21-24] Moreover, the measured oxidation current at 250 μm away from the human mucosal surface (> 4 nA) appears greater than that measured in guinea pig mucosa suggesting that DMEs are stable in regions with possible greater serotonin concentrations.[46] Figure 9B shows cyclic voltammetric *i-E* curves recorded for a typical DME new and after one year of multiple tissue measurements. During the one-year span, the electrode was used for experimentation and stored under laboratory atmosphere conditions. The only pretreatment periodically applied to the DME was a 20-min soak in ultrapure (distilled and stored over activated carbon) isopropanol. There was a minor shift on the peak oxidation potential positively by ~0.22 V over time, but the peak current remained unchanged demonstrating that DMEs are resistant to significant deactivation when exposed to gut tissue and air for an extended time. For the few cases in which significant fouling was observed, *in situ* electrochemical pretreatment is an effective means for DME reactivation.[54]
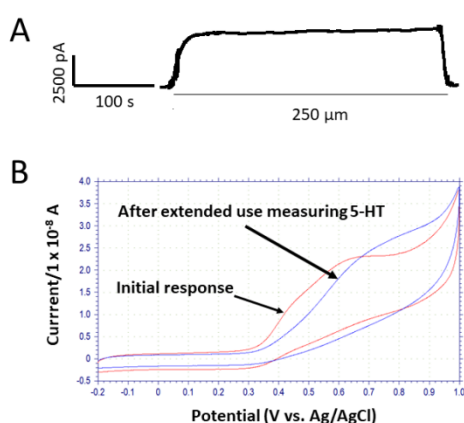
Figure 9. (A) Continuous amperometric *i-t* recording of the stable serotonin oxidation current at a distance of 250 μm over a 5-min period. Detection potential = 0.8 V vs. Ag/AgCl. The shearing force of the buffer flow stimulates mechanosensitive receptors expressed by mucosal EC cells; a process that evokes serotonin release. (B) Cyclic voltammetric *i-E* curves were made in a 10 μmol L^{-1} serotonin in Krebs buffer before and after extended tissue exposure (~3 months).

4. Discussion

The results demonstrate that DMEs can be used for sufficiently sensitive, reproducible, and stable measurements of serotonin released from EC cells in the mucosa of the human jejunum. The results also show, as expected, that serotonin oxidation currents can be manipulated by blockade of SERT. Fluoxetine is a known SSRI in human and animal models. To date, there has been no report on the use of DMEs for *in vitro* measurements in human intestinal tissues.

The electrochemical measurement with a DME and the current-approach curve data analysis provides key information on the serotonin signalling mechanism, where steady-state levels are observed. The results portend that the method could be used to provide vital information on neurochemical signalling differences between normal and diseased tissue, as well as for assessing the efficacy of pharmacological agents in GI tissue.

Marcelli and Patel developed a model for recording and analyzing continuous amperometric current data with distance to better understand serotonin release and uptake dynamics in the intestinal mucosa.[46,47] Past research using continuous amperometry to study serotonin release and uptake in the intestinal mucosa involved measurements at either one distance[21] from the mucosa or when touching the mucosa with the microelectrode.[61-63] These measurements may either mask true changes in serotonin release and uptake or are at risk of electrode response stability loss due to biofouling, respectively. The serotonin oxidation current temporally measured depends on a balance between the rate of neurotransmitter released from EC cells nearby the recording microelectrode and the rate of recapture by SERT uptake. In most studies using CA to measure serotonin in GI mucosa, the current measured at one electrode distance represents a combination of information on neurotransmitter release and uptake, and only provides ambiguous descriptions of serotonin release or uptake. Electrodes were coated with the polymer film Nafion™ to prevent electrode fouling in previous studies that required the electrode to touch the mucosal surface.[61,62] However microelectrodes treated with Nafion™ have prolonged response times when subjected to rapidly changing concentrations of serotonin *in vitro*[63] while being protected from biofouling. DMEs are resistant to biofouling and can be used to rapidly record temporally

changing serotonin oxidation current measurements over range of electrode-tissue distances. Hanssen et al. have recently reviewed strategies for preventing biofouling.[66] While no direct comparison studies were performed in gut tissues, it appears that the DMEs possess comparable biofouling resistance to other sp^2-bonded nanocarbon electrodes using in neurochemical analysis: carbon nanotubes[67,68], nanoyarn[69], and fuzzy graphene microelectrodes.[70]

Conclusions

The key findings from this study are that (i) diamond microelectrodes provide excellent response performance characteristics for serotonin oxidation *in vitro* in the human jejunum, (ii) the dynamics of serotonin release and uptake in human jejunum tissue can be effectively studied using current-approach curves in the continuous amperometric measurement mode, and (iii) SERT function in these tissues was not impaired by the tissue harvesting, transport and mounting procedures and can be manipulated by fluoxetine.

Author Contributions

MF conducted the experiments, data analysis and contributed to the writing of the manuscript. JJG and GMS contributed to the design of the experiments, review of the experimental results, and writing of the manuscript. All authors approved this submission.

Conflicts of interest

There are no conflicts to declare.

Acknowledgements

References

1. G. M. Swain and R. Ramesham, *Anal. Chem*. 1992, **65**, 345-351.

2. A. Argoitia, H. B. Martin, E. J. Rozak, U. Landau and J. C. Angus, *MRS Advances* 1995, **416**, 349-354.

3. M. C. Granger, J. Xu, J. W. Strojek and G. M. Swain, *Anal. Chim. Acta* 1999, **397**, 145-161.

4. J. V. Macpherson, *Phys. Chem. Chem. Phys*. 2015, **17**, 2935-2949.

5. M. C. Granger and G. M. Swain, *J. Electrochem. Soc*. 1999, **146**, 4551-4558.

6. S. Wang, V. M. Swope, J. E. Butler, T. Feygelson and G. M. Swain, *Diam. Relat. Mater*. 2009, **18**, 669-677.

7. D. Y. Kim, J. Wang, J. Yang, H. W. Kim and G. M. Swain, *J. Phys. Chem. C* 2011, **115**, 10026-10032.

8. R. Jarosova, P. M. Bezerra De Sousa, C. Munson and G. M. Swain, *Phys. Status Solidi A* 2016, **213**, 2087-2098.

9. S. Y. Tan, R. A. Lazenby, K. Bano, J. Zhang, A. M. Bond, J. V. Macpherson and P. R. Unwin, *Phys. Chem. Chem. Phys*. 2017, **19**, 8726-8734.

10. S. Haymond, G. T. Babcock and G. M. Swain, *Electroanal*. 2003, **15**, 249-253.

11. G. Pastor-Moreno and D. J. Riley, *Electrochim. Acta* 2002, **47**, 2589-2595.

12. R. Jarošová, K. Bhardwaj and G. M. Swain, *J. Electroanal. Chem.* 2020, **875**, 114744.

13. C. Zhao, G. Burrel, A. A. Torriero, F. Separovic, N. F. Dunlop, D. R. MacFarlane and A. M. Bond, *J. Phys. Chem. B* 2008, **112**, 6923-6936.

14. H. Dong, S. Wang, J. J. Galligan and G. M. Swain, *Front. Biosci*. 2011, **3**, 518-540.

15. F. S. Manciu, Y. Oh, A. Barath, A. E. Rusheen, A. Z. Kouzani, D. Hodges, J. Guerrero, J. Tomshine, K. H. Lee and K. E. Benne, *Materials* 2019, **12**, 3186.

16. E. K. Purcell, M. F. Becker, Y. Guo, S. A. Hara, K. A. Ludwig, C. J. McKinney, E. M. Monroe, R. Rechenberg, C. A. Rusinek, A. Saxena, J. R. Siegenthaler, C. E. Sortwell, C. H. Thompson, J. K. Trevathan, S. Witt and W. Li, *Micromachines* 2021, **12**, 128.

17. M. L. Huffman and B. J. Venton, *Analyst* 2009, **134**, 18-24.

18. J. Park, J. J. Galligan, G. D. Fink and G. M. Swain, *Anal. Chem*. 2006, **78**, 6756-6764.

19. J. Park, J. J. Galligan, G. D. Fink and G. M. Swain, *J. Physiol*. 2007, **584**, 819-834.

20. J. Park, V. Quaiserová-Mocko, B. A. Patel, M. Novotný, A. Liu, X. Bian, J. J. Galligan and G. M. Swain, *Analyst* 2008, 133, 17-24.

21. B. A. Patel, X. Bian, V. Quaiserová-Mocko, J. J. Galligan and G. M. Swain, *Analyst* 2007, **132**, 41-47.

22. B. A. Patel, X. Dai, J. E. Burda, H. Zhao, G. M. Swain, J. J. Galligan and X. Bian, *Neurogastroenterol. Motil.* 2010, **22**, 909-918.

23. H. Zhao, X. Bian, J. J. Galligan and G. M. Swain, *Diam. Relat. Mater.* 2010, **19**, 182-185.

24. J. J. Galligan, B. A. Patel, S. P. Schneider, H. Wang, H. Zhao, M. Novotny, X. Bian, R. Kabeer, D. Fried and G. M. Swain, *Neurogastroenterol. Motil.* 2013, **25**, e373-381.

25. B. A. Patel, J. J. Galligan, G. M. Swain and X. Bian, *Neurogastroenterol. Motil.* 2008, **20**, 1243-1250.

26. M. Z. Wrona and G. Dryhurst*, J. Pharm. Sci.* 1988, **77**, 911-917.

27. M. Z. Wrona and G. Dryhurst*, J. Electroanal. Chem.* 1990, **278**, 249-267.

28. M. Poon and R. L. McCreery, *Anal. Chem.* 1987, **59**, 1615-1620.

29. J. E. Baur, E. W. Kristensen, L. J. May, D. J. Wiedemann and R. M. Wightman, *Anal. Chem*. 1988, **60**, 1268-1272.

30. G. Dryhurst, *Chem. Rev.* 1990, **90**, 795-811.

31. M. Z. Wrona and G. Dryhurst, *Bioorg. Chem.* 1990, **18**, 291-317.

32. K. Bhardwaj, F. Parvis, Y. Wang, G. J. Blanchard and G. M. Swain, *Langmuir* 2020, **36**, 5717-5729.

33. S. Kasahara, T. Ogose. N. Ikemiya, T. Yamamoto, K. Natsui, Y. Yokota, R. A. Wong, S. Iizuka, N. Hoshi, Y. Tateyama, Y. Kim, M. Nakamur and Y. Einaga, *Anal. Chem*. 2019, **91**, 4980-4986.

34. C. Hébert, J. Warnking, A. Depaulis, L. A. Garçon, L. M. Mermoux, D. Eon, P. Mailley and F. Omnès, *Mater. Sci. Eng. C Mater. Biol. Appl.* 2015, **46**, 25-31.

35. Y. T. Wong, A. Ahnood, M. I. Maturana, W. Kentler, K. Ganesan, D. B. Grayden, H. Meffin, S. Prawer, M. R. Ibbotson and A. N. Burkitt, *Front. Bioeng. Biotechnol*. 2018, **6**, 85.

36. J. M. Halpern, S. Xie, G. P. Sutton, B. T. Higashikubo, C. A. Chestek, H. Lu, H. J. Chiel and H. B. Martin, *Diam. Relat. Mater*. 2006, **15**, 183-187.

37. A. Suzuki, T. A. Ivandini, K. Yoshimi, A. Fujishima, G. Oyama, T. Nakazato, N. Hattori, S. Kitazawa and Y. Einaga, *Anal. Chem.* 2007, **79**, 8608-8615.

38. K. Yoshimi, Y. Naya, M. Mitani, T. Kato, M. Inoue, S. Natori, T. Takahashi, A. Weitemier, N. Nishikawa, T. McHugh, Y. Einaga and S. Kitazawa, *Neurosci. Res.* 2011, **71**, 49-62.

39. K. E. Bennet, J. R. Tomshine, H. K. Min, F. S. Manciu, M. P. Marsh, S. B. Paek, M. L. Settell, E. N. Nicolai, C. D. Blaha, A. Z. Kouzani, S. Y. Chang and K. H. Lee, *Front. Hum. Neurosci.* 2016, **10**, 102.

40. Y. S. Singh, L. E. Sawarynski, H. M. Michael, R. E. Ferrell, M. A. Murphey-Corb, G. M. Swain, B. A. Patel and A. M. Andrews, *ACS Chem. Neurosci.* 2010, **1**, 49-64.

41. A. Hanawa, G. Ogata, S. Sawamura, K. Asai, S. Kanzaki, H. Hibino and Y. Einaga, *Anal. Chem*. 2020, **92**, 13742-13749.

42. S. Fierro, M. Yoshikawa, O. Nagano, K. Yoshimi, H. Saya and Y. Einaga, *Sci. Rep.* 2012, **2**, 901.

43. B. Fan, C. A. Rusinek, C. H. Thompson, M. Setien, Y. Guo, R. Rechenberg, Y. Gong, A. J. Weber, M. F. Becker, E. Purcell, W. Li, *Microsyst. Nanoeng*. 2020, **6**, 42

44. A. Y. Chang, G. Dutta, S. Siddiqui and P. U. Arumugam, *ACS Chem. Neurosci.* 2019, **10**, 313-322.

45. P. Puthongkham and B. J. Venton, *Analyst* 2020, **145**, 1087-1102.

46. G. Marcelli and B. A. Patel, *Analyst* 2010, **135**, 2340-2347.

47. G. Marcelli and B. A. Patel, *Conf. Proc. IEEE Eng. Med. Biol. Soc. 2008*, 5548-5551.

48. S. Diwakarla, L. J. Fothergill, J. Fakhry, B. Callaghan and J. B. Furness, *Neurogastroenterol. Motil.* 2017, **29**, 10.1111/nmo.13101

49. M. D. Gershon, *Curr. Opin. Endocrinol. Diabetes. Obes*. 2013, **20**, 14-21.

50. M. D. Gershon and J. Tack, *J. Gastroenterol.* 2007, **132**, 397-414.

51. A. Sikander, S. V. Rana and K. K. Prasad, *Clin. Chim. Acta.* 2009, **403**, 47-55.

52. J. B. Cooper, S. Pang, S. Albin, J. Zheng and R. M. Johnson, *Anal. Chem*. 1998, **70**, 464-467.

53. J. Cvacka, V. Quaiserová, J. Park, Y. Show, A. Muck Jr. and G. M. Swain, *Anal. Chem.* 2003, **75**, 2678-2687.

54. B. Duran, R. F. Brocenschi, M. France, J. J. Galligan and G. M. Swain, *Analyst* 2014, **139**, 3160-3166.

55. M. Fhaner, H. Zhao, X. Bian, J. J. Galligan and G. M. Swain, *Diam. Relat. Mater.* 2011, 20, 75-83.

56. A. C. Ferrari and J. Robertson, *Phys. Rev. B*. 2001, **63,** 121405-1.

57. J. Birrell, J. E. Gerbi, O. Auciello, J. M. Gibson, J. Johnson and J. A. Carlisle, *Diam. Rel. Mater*. 2005, **14**, 86-92.

58. J. Wagner, C. Wild and P. Koidl, *Appl. Phys. Lett*. 1991, **59**, 779-781.

59. B. P. Jackson, S. M. Dietz and R. M. Wightman, *Anal. Chem.* 1995, **67**, 1115-1120.

60. A. Linan-Rico, F. Ochoa-Cortes, A. Beyder, S. Soghomonyan, A. Zuleta-Alarcon, V. Coppola and F. L. Christofi, *Front. Neurosci.* 2016, **10**, 564.

61. P.P. Bertrand, X. Hu, J. Mach and R. L. Bertrand, *Am. J. Physiol. Gastrointest. Liver Physiol.* 2008, **295**, G1228-1236.

62. R. L. Bertrand, S. Senadheera, I. Markus, L. Liu, L. Howitt, H. Chen, T. V. Murphy, S. L. Sandow and P. P. Bertrand, *Endocrinology* 2011, **152**, 36-47.

63. R. L. Bertrand, S. Senadheera, A. Tanoto, K. L. Tan, L. Howitt, H. Chen, T. V.Murphy, S. L. Sandow, L. Liu and P. P. Bertrand, *Am. J. Physiol. Gastrointest. Liver Physiol.* 2012, **303**, G424-434.

Analyst

64. H. Schwörer and G. Ramadori, *Naunyn Schmiedebergs Arch Pharmacol.* 1998, 357, 548-552.

65. K. Racké, A. Reimann, H. Schwörer and H. Kilbinger, *Behav. Brain Res.* 1996, **73**, 83-87.

66. B. L. Hanssen, S. Siraj and D. K. Y. Wong, *Rev. in Anal. Chem*. 2016, **35**, 1-28.

67. A. Fagan-Murphy, M. C Allen and B. A. Patel, *Electrochim. Acta* 2015, **152**, 249-254.

68. C. Yang, E. Trikantzopoulos, C. B. Jacobs and B. J. Venton, *Anal Chim Acta*. 2017, **965**, 1-8.

69. A. Mendoza, T. Asrat, F. Liu, P. Wonnenberg and A. G. Zestos, *Sensors* 2020, **20**, 1173.

70. E. Castagnola, R. Garg, S. K. Rastogi, T. Cohen-Karni and X. T. Cui, *Biosens. Bioelectron*. 2021, **191**, 113440.